JOURNAL OF GEOPHYSICAL RESEARCH, VOL. 113, A06205, doi:10.1029/2007JA012752, 2008

Particle precipitation during ICME-driven and CIR-driven geomagnetic storms

N. Longden,[1] M. H. Denton,[1] and F. Honary[1]

Received 24 August 2007; revised 23 November 2007; accepted 28 January 2008; published 5 June 2008.

[1] Interplanetary coronal mass ejections (ICME) and corotating interaction regions (CIR) alter the parameters of the solar wind and interplanetary magnetic field (IMF) that affect conditions in the Earth's magnetosphere and particle precipitation in the auroral zone. We perform a superposed epoch study of the effects of ICME-dominated and CIR-dominated solar wind on particle precipitation during geomagnetic storms. We use data from a set of 38 CIR events and 33 ICME events. Particle precipitation is inferred from cosmic noise absorption (CNA) recorded by the riometer at Abisko. The electron flux intensity at geosynchronous orbit close to the location of the riometer is taken from the synchronous orbit particle analyzer (SOPA) onboard the Los Alamos National Laboratory (LANL) satellite LANL-01A. The results show that mean CNA is more intense during the main phase of ICME-driven storms. In contrast, mean CNA remains elevated for a much longer period during CIR-driven storms indicating prolonged periods of particle precipitation. Enhanced CNA over a sustained period of time is observed during CIR-driven storms that are categorized as only weak or moderate in terms of the response that they drive in the Dst index (Dst >-100 nT). This result indicates that events which may be considered geomagnetically ineffective have a significant effect on particle precipitation in the auroral zone. The elevated CNA observed during CIR-driven storms is accompanied by elevated electron flux intensity, measured at geosynchronous orbit, over all channels in the 50–500 keV range at all local times.

Citation: Longden, N., M. H. Denton, and F. Honary (2008), Particle precipitation during ICME-driven and CIR-driven geomagnetic storms, *J. Geophys. Res.*, *113*, A06205, doi:10.1029/2007JA012752.

1. Introduction

[2] Interaction between the solar wind and the Earth's magnetosphere can cause disturbances in the geomagnetic field. The solar wind parameters that affect the level of geomagnetic activity are the solar wind velocity (**v**) and the southward oriented component of the interplanetary magnetic field (IMF) in GSM coordinates (B_s) [e.g., *Gonzalez and Tsurutani*, 1987; *Gosling et al.*, 1991; *Gonzalez et al.*, 1999; *Borovsky and Denton*, 2006; *Tsurutani et al.*, 2006, and references therein].

[3] Two solar wind structures have been identified as the important drivers of geomagnetic storms; interplanetary coronal mass ejections (ICME) and corotating interaction regions (CIR) [e.g., *Richardson et al.*, 2000].

[4] ICMEs are the interplanetary (IP) counterpart of massive eruptions of magnetized solar plasma. Typically, an ICME is composed of an interplanetary shock wave, a sheath region of compressed solar wind and an ejecta [e.g., *Gopalswamy*, 2003]. The configuration of the magnetic field in the sheath and the ejecta can lead to enhanced B_s. Almost all shocks observed at 1 astronomical unit (AU) are associated with an ICME [*Sheeley et al.*, 1985], a feature shown to enhance geomagnetic effects [*Gosling et al.*, 1991]. However, not all ICMEs are sufficiently fast to drive a shock [*Gosling et al.*, 1991]. In this paper, geomagnetic storms driven by any combination of an ICME shock, sheath or ejecta are termed ICME driven storms.

[5] CIRs are regions of compressed magnetic field and plasma that result from interaction between high-speed and slow-speed solar wind streams [e.g., *Tsurutani et al.*, 1995, 2006]. The fast-solar wind streams typically have speeds of $\sim$750 to 800 kms^{-1}, and emanate from coronal holes, whereas slow-speed streams typically have speeds of $\sim$300 to 400 kms^{-1}, and originate from the streamer belt region [e.g., *Tsurutani et al.*, 2006]. As coronal holes can persist for longer than the rotation period of the Sun, the high-speed streams may reoccur with a frequency of $\sim$27 days. The term CIR is applied to the interaction region and the period of high solar wind speed which follows each interaction region in this paper.

[6] The likelihood of the solar wind being dominated by either an ICME or CIR structure is dependent on the level of solar activity [e.g., *Tsurutani et al.*, 1995; *Gonzalez et al.*, 1999; *Richardson et al.*, 2000, 2001]. CIRs usually

[1]Department of Communication Systems, Lancaster University, Lancaster, UK.

0148-0227/08/2007JA012752$09.00

occur during the declining phase of solar activity. ICMEs occur throughout the entire solar cycle but are more frequent in the period around solar maximum [e.g., *St. Cyr et al.*, 2000].

[7] Features of geomagnetic storms have been observed to exhibit different characteristics dependent on the solar wind driver [e.g., *Tsurutani et al.*, 2006; *Borovsky and Denton*, 2006; *Denton et al.*, 2006]. CIR-driven storms are more likely to occur following an extended period of geomagnetic calm than ICME-driven storms [*Borovsky and Denton*, 2006, and references therein] where a period of calm is defined as $Kp \leq 1^+$ over one to two days. *Borovsky and Denton* [2006] have shown that ICMEs have a greater influence over the ring current than CIRs while CIRs have the greater influence over magnetospheric convection, which can measured using the Kp index [*Bartels et al.*, 1939; *Thomsen*, 2004]. The density and temperature of particles at geosynchronous orbit also exhibit different profiles during storms depending on the solar wind driver [*Denton et al.*, 2006].

[8] One manifestation of geomagnetic activity is the precipitation of particles trapped in the magnetosphere into the ionosphere in the auroral zone. Variation of ionospheric characteristics can have implications for High Frequency (HF) communication [e.g., *Kavanagh et al.*, 2004]. Precipitation of energetic electrons (E > 30 keV) in the D-region of the ionosphere can be inferred through measurement of the level of absorption of cosmic radio noise (CNA) during propagation through the ionosphere by ground-based riometers.

[9] The passage of geomagnetically effective ICMEs and CIRs can provide a number of driving mechanisms for enhanced electron precipitation [e.g., *Longden et al.*, 2007]. Substorms, a feature common to all geomagnetic storms [e.g., *Gonzalez et al.*, 1994] are known to drive precipitation [e.g., *Hargreaves et al.*, 1975; *Ranta et al.*, 1981]. This precipitation is linked to the injection of particles at the time of substorm onset, with CNA observed around local midnight at the time of the initial injection and CNA observed in the local morning as the injected particles drift and harden [e.g., *Stauning*, 1996]. Precipitation can also be caused by rapid compression of the magnetosphere resulting from changes in the incident solar wind pressure (P_{dyn}) [*Brown et al.*, 1961, 1972; *Brown and Driatsky*, 1973; *Perona*, 1972]. Changes in P_{dyn} can be driven by solar wind features such as IP shocks and regions of high density. *Kavanagh et al.* [2004] have shown that CNA is dependent on the same solar wind parameters as geomagnetic activity, namely **v** and B_s. CNA has been observed to reoccur with a 27 day period during the declining phase of solar activity [*Hultqvist*, 1966 and references therein] implying a link between CIR activity and CNA.

[10] The aim of the current study is to compare the magnetospheric response in terms of electron precipitation during ICME-driven and CIR-driven storms. We perform a superposed epoch analysis on riometer data during 33 ICME-driven and 38 CIR-driven storms. A broad correlation has previously been shown between energetic electron flux at geosynchronous orbit and CNA during substorms [e.g., *Parks et al.*, 1968; *Baker et al.*, 1981] and riometer measurements have been used to identify substorm activity [*Spanswick et al.*, 2007]. We use electron flux intensity data from the synchronous orbit particle analyzer (SOPA) instrument [*Belian et al.*, 1992] onboard one of the Los Alamos National Laboratory (LANL) satellites at geosynchronous orbit to enable investigation of the relationship between this and CNA throughout the development of a storm.

2. Instrumentation

[11] Energetic electron precipitation is inferred from CNA data from the widebeam riometer located at Abisko, Sweden (68.40°N, 18.90°E geographic). This riometer operates at 30 MHz and is part of the chain of riometers operated by the Sodankylä Geophysical Observatory (SGO). Between 2000 and 2006, the riometer at Abisko mapped to an L shell of ~5.81 to ~5.85 and had a magnetic latitude in the range ~65.30°N to ~65.37°N. Magnetic latitudes are given the Corrected Geomagnetic (CGM) coordinate system using the International Geomagnetic Reference Field (IGRF) model [e.g., *Maus et al.*, 2005].

[12] Electron flux intensity data are taken from the SOPA instrument onboard the LANL-01A satellite located in geosynchronous orbit. LANL-01A was located at a geographic longitude between 7.6°E and 9°E during these events and ostensibly maps to an L shell of 6.6. During 2000 to 2006, the footprint of a geomagnetic field line mapped from the equator at 6.6 R_E at the longitude of the LANL-01A satellite using the Tsyganenko 89C model [*Tsyganenko*, 1995] was around 67°N. The SOPA instrument records electrons with energies in the range 50 keV to ~ 26 MeV over 16 energy channels.

[13] Observations of the solar wind conditions at the L1 point during the events are taken from the magnetic fields experiment (MAG) instrument [*Smith et al.*, 1998] and the Solar Wind Electron Proton Alpha Monitor (SWEPAM) instrument [*McComas et al.*, 1998] onboard the Advanced Composition Explorer (ACE) satellite. The parameters selected to indicate solar wind conditions were v_x and B_z (GSM), due to their influence on the strength of the interplanetary convective field, and v_y (a measure of the east-west velocity of the solar wind. A change from westerly direction (−) to an easterly direction (+) is a typical signature of a CIR event.

3. Data Analysis

3.1. Event Selection

[14] Candidate ICME events were initially selected from the list of ICMEs compiled by *Cane and Richardson* [2003]. This list covers the period from 1996 to 2002. Data are available from the LANL-01A satellite from October 2000 and events occurring before this time were not used in this study. Additional ICME events occurring between 2002 and 2006 were identified from solar wind plasma and IMF data. Candidate CIR events were selected from the list used by *Denton et al.* [2006], covering the period of 1993 to 2005. These events were selected from a list of east/west deflections in the solar wind [R. McPherron, private communication], with additions based on direct examination of solar wind data. Again, events occurring prior to the coverage of LANL-01A were discarded. ICME and CIR events were also discarded when there was incomplete data

Table 1. Frequency of Occurrence of Storm Intensity by Solar Wind Driver

Storm Intensity	Range of $\hat{D}st$		CIR Events	ICME Events
Weak		$\hat{D}st > -50$ nT	22	10
Moderate	$-50 \geq$	$\hat{D}st > -100$ nT	15	9
Intense	$-100 \geq$	$\hat{D}st > -240$ nT	1	12
Super		$\hat{D}st \leq -240$ nT	0	2

coverage during the event, when a subsequent event was observed within 72 h of the time of the onset of the initial event or when no clear minimum in the Dst index was observed following the onset of the event. Applying these criteria resulted in a set of 33 ICME events from 2000 to 2006 and a set of 38 CIR events from 2003 to 2005 for analysis. The prehistory of the solar wind or background conditions in the magnetosphere were not considered.

3.2. Epoch Analysis

[15] In this study, geomagnetic activity is inferred from three indices; Dst, Kp and SYM-H. Dst is considered to be a measure of intensity of the ring current [e.g., *Grafe*, 1999, and references therein] and can be used to categorize storm intensity [e.g., *Gonzalez et al.*, 1994]. The Kp index can also be used to categorize storm intensity [e.g., *Gosling et al.*, 1991] and is a proxy for the strength of magnetospheric convection. The SYM-H index is a similar measure to the Dst index but has a 1 min resolution [e.g., *Wanliss and Showalter*, 2006]. The higher resolution means that the SYM-H index can be used to investigate geomagnetic activity on a smaller temporal scale, such as sudden impulses (SI) [e.g., *Takeuchi et al.*, 2002].

[16] For each event, the Dst index was inspected to identify the first clear minimum value following the arrival of the solar wind structure at the magnetosphere. The time of arrival can be estimated from the solar wind speed and the time of initial observation by the ACE satellite [e.g., *Khan and Cowley*, 1999] and is typically of the order of an hour for ICME and CIR events. Following *Denton et al.* [2006] the first minimum in Dst was used as the zero epoch for the event. Data were taken from 24 h prior to and 72 h following the zero epoch to cover the period from storm onset through to recovery. Storm intensity was determined from the lowest value of Dst observed throughout the duration of the storm. Table 1 shows a summary the number of storms at each intensity level according to driving structure. As storms may experience growth in more than one phase [e.g., *Kamide et al.*, 1998], the time of zero epoch is not necessarily the time of minimum Dst. SOPA data with a temporal resolution of 10 s and ACE data with a temporal resolution of 64 s were used. Linear interpolation was applied to the SOPA and ACE data to ensure consistent timing for these data sets between events.

[17] We have performed the analysis using data from storms of all intensities and then from storms of weak to moderate intensity only, to enable comparison of precipitation due to the solar wind driver during similar storm conditions.

[18] Mean values as a function of epoch time were calculated at the sampling rate for each data set for particle precipitation, solar wind parameters and geomagnetic indices. An estimate for solar wind P_{dyn} was obtained from the proton number density and solar wind velocity data from the ACE satellite.

4. Results

[19] The results of the superposed epoch analysis are shown in Figures 1 and 2. Figure 1 shows the results of the study when data during storms of all intensities are considered and Figure 2 shows the results for storms of weak and moderate intensity only. In both figures, the panels show, from top to bottom, the mean electron flux intensity of 50–75 keV electrons from the LANL-01A satellite, mean absorption from the Abisko riometer, mean v_x, mean v_y and mean IMF B_z from the ACE satellite, mean P_{dyn} calculated from ACE data, and mean SYM-H, Kp and Dst indices as a function of epoch time. A dashed line indicating a value of zero is shown for v_y and B_z to highlight zero crossings. Figures 3 and 4 show the mean data from the epoch analysis study for CIR-driven and ICME-driven storms of all intensities respectively with ±1 standard deviation indicated by the dashed lines.

[20] From Figure 1b, mean CNA from the Abisko riometer during ICME-driven storms of all intensities shows an increase from ~10 h prior to the zero epoch. Two clear peaks are also evident in this data; the first ~1 h prior to the zero epoch and the second ~5 h following the zero epoch. Following the second peak, mean CNA is observed to decay to levels below that observed prior to the zero epoch. Mean CNA during CIR-driven storms also shows an increase from ~10 h prior to the zero epoch. This CNA increases gradually and then remains elevated throughout the period of the study following the zero epoch.

[21] From Figure 4b, it can be seen that the standard deviation in the magnitude of CNA in ICME events decreases ~14 h after the zero epoch, around the time that the mean value is seen to decrease. This is consistent with less intense precipitation at this time as the mean value of CNA and the deviation of intensities away from this mean are both reduced. The standard deviation in CNA during CIR events (Figure 3b) does not show a marked decrease at a given time in the development of the storm, also consistent with enhanced precipitation following the zero epoch.

[22] The most intense CNA is observed when ICMEs are the dominant structure in the solar wind. However, CNA related to the passage of a CIR exceeds that related to ICMEs over a sustained period of time. As a result of the sustained enhancement of CNA, total mean absorption during CIR-driven storms slightly exceeds total mean absorption during ICME-driven storms over the four day period of the study.

[23] When mean CNA during weak and moderate storms only is considered (Figure 2b), the profile during CIR events is largely unchanged. This is unsurprising as only 1 of the 38 events did not generate storms of these intensities. However, the 19 ICMEs that drove a weak or moderate storm produced mean CNA somewhat different to that observed during ICME-driven storms of all intensities. Mean CNA is lower in magnitude during the lower intensity storms throughout the period of the study. Two peaks around 2 h prior to and 5 h following the zero epoch can still be identified but numerous additional peaks of equal

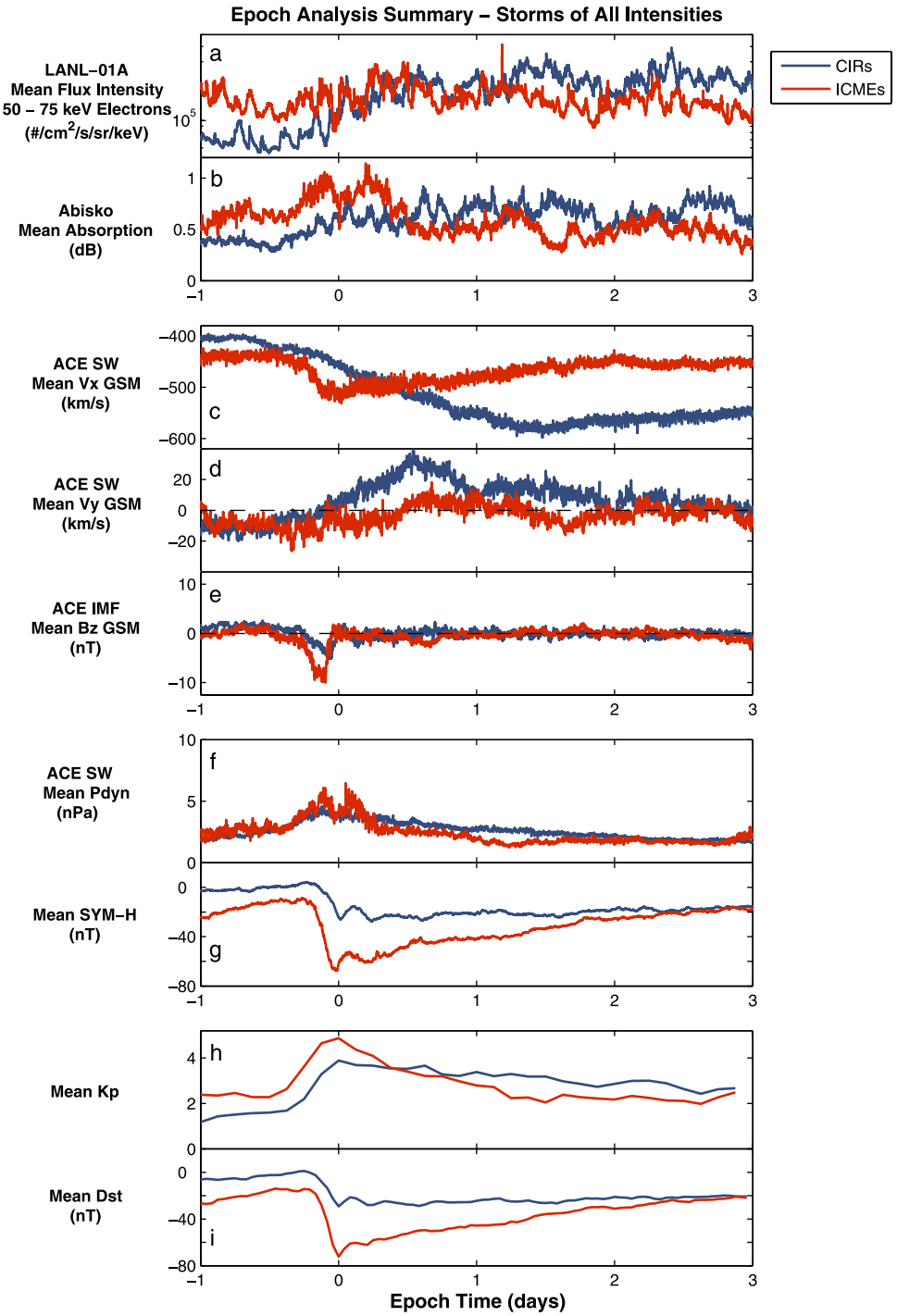

Figure 1. Superposed epoch time series of data for the set of 38 CIR-driven storms and 33 ICME-driven storms. From (a) to (i), the panels show mean electron flux intensity for electrons with energies in the range 50–75 keV from the LANL-01A satellite, mean CNA from the Abisko riometer, mean solar wind velocity in the X and Y direction (GSM), mean IMF B_z (GSM), mean solar wind P_{dyn}, mean SYM-H, mean Kp and mean Dst. The zero epoch is the time of the first clear minimum in Dst for each event.

magnitude can be observed at other times in the study. Also, the peak intensity of CNA during ICME-dominant solar wind is of similar magnitude to the peak CNA during CIR-dominant solar wind.

[24] CIRs have a consistent structure; slow solar wind is followed by an interaction region which is then followed by a period of fast solar wind. These results highlight the fact that typical CIR-Earth interactions are similar in nature. In contrast, ICME-Earth interactions are all very different in nature since they depend on the size, structure, density etc. of the associated solar wind structure.

[25] The general trend in mean 50–75 keV electron flux intensity closely follows the trend in mean absorption at Abisko during CIR-driven storms. Mean 50–75 keV elec-

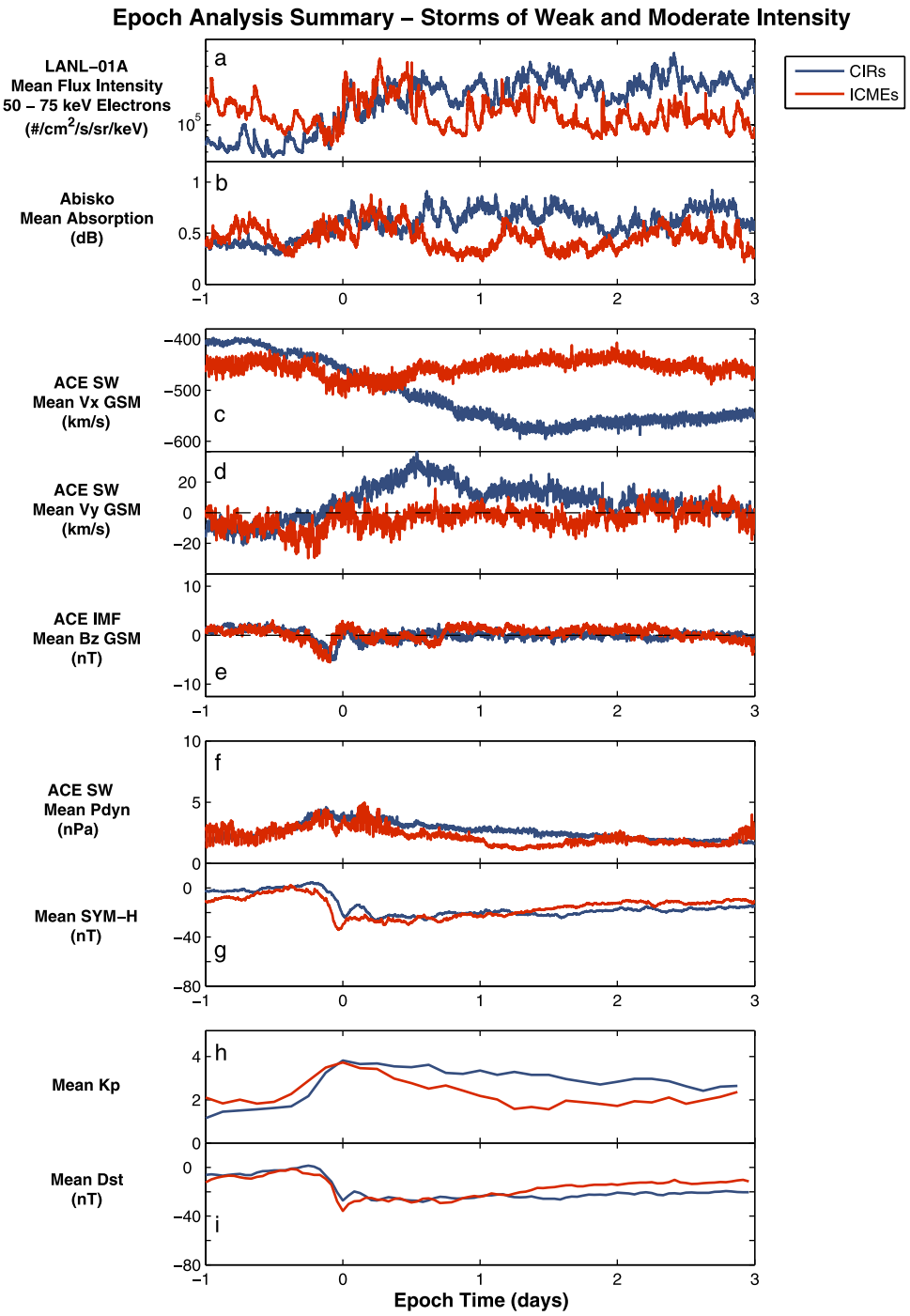

Figure 2. Superposed epoch time series of data for the set of 37 CIR-driven storms and 19 ICME-driven storms of weak and moderate intensity (Dst >−100 nT). From (a) to (i), the panels show mean electron flux intensity for electrons with energies in the range 50–75 keV from the LANL-01A satellite, mean CNA from the Abisko riometer, mean solar wind velocity in the X and Y direction (GSM), mean IMF B_z (GSM), mean solar wind P_{dyn}, mean SYM-H, mean Kp and mean Dst. The zero epoch is the time of the first clear minimum in Dst for each event.

tron flux intensity is initially low, gradually rising prior to the zero epoch and remaining high throughout the rest of the period of the study. The similarity is less pronounced during ICME-driven storms although is still somewhat elevated. However, when storms are considered individually, the significant correlation between CNA and 50–75 keV electron flux intensity ranges from highly correlated (r > 0.8) to uncorrelated (r ≈ 0) over the four day period for both CIR- and ICME-driven storms. It should be noted that geomagnetic activity can alter the mapping of equatorial field lines [e.g., *Tsyganenko*, 1995], affecting the spatial separation between the riometer at Abisko and the LANL-01A satellite

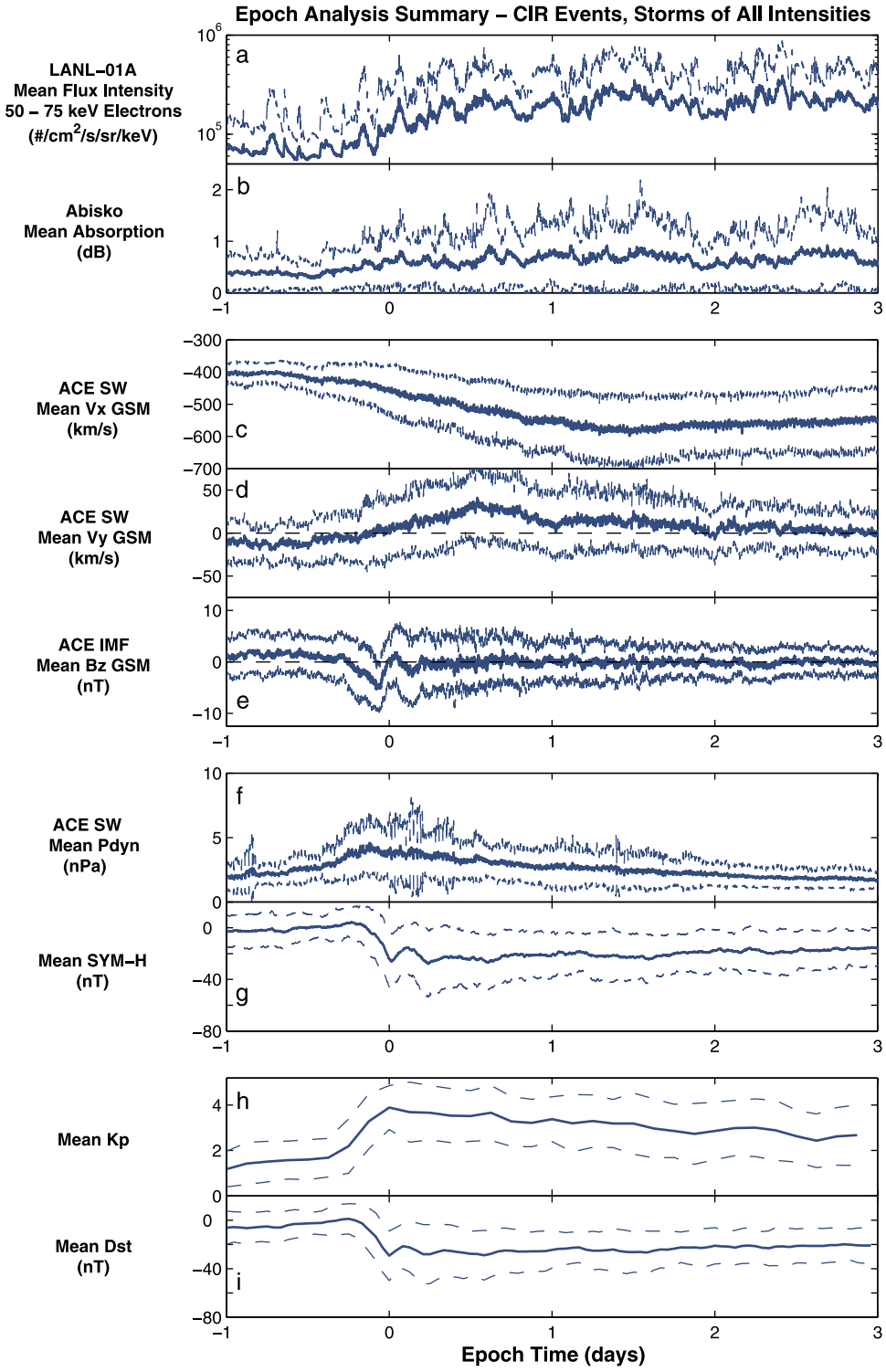

Figure 3. Superposed epoch time series of data for the set of 38 CIR-driven storms. ±1 Standard deviation from the mean is indicated for each data set. From (a) to (i), the panels show mean electron flux intensity for electrons with energies in the range 50–75 keV from the LANL-01A satellite, mean CNA from the Abisko riometer, mean solar wind velocity in the X and Y direction (GSM), mean IMF B_z (GSM), mean solar wind P_{dyn}, mean SYM-H, mean Kp and mean Dst. The zero epoch is the time of the first clear minimum in Dst for each event.

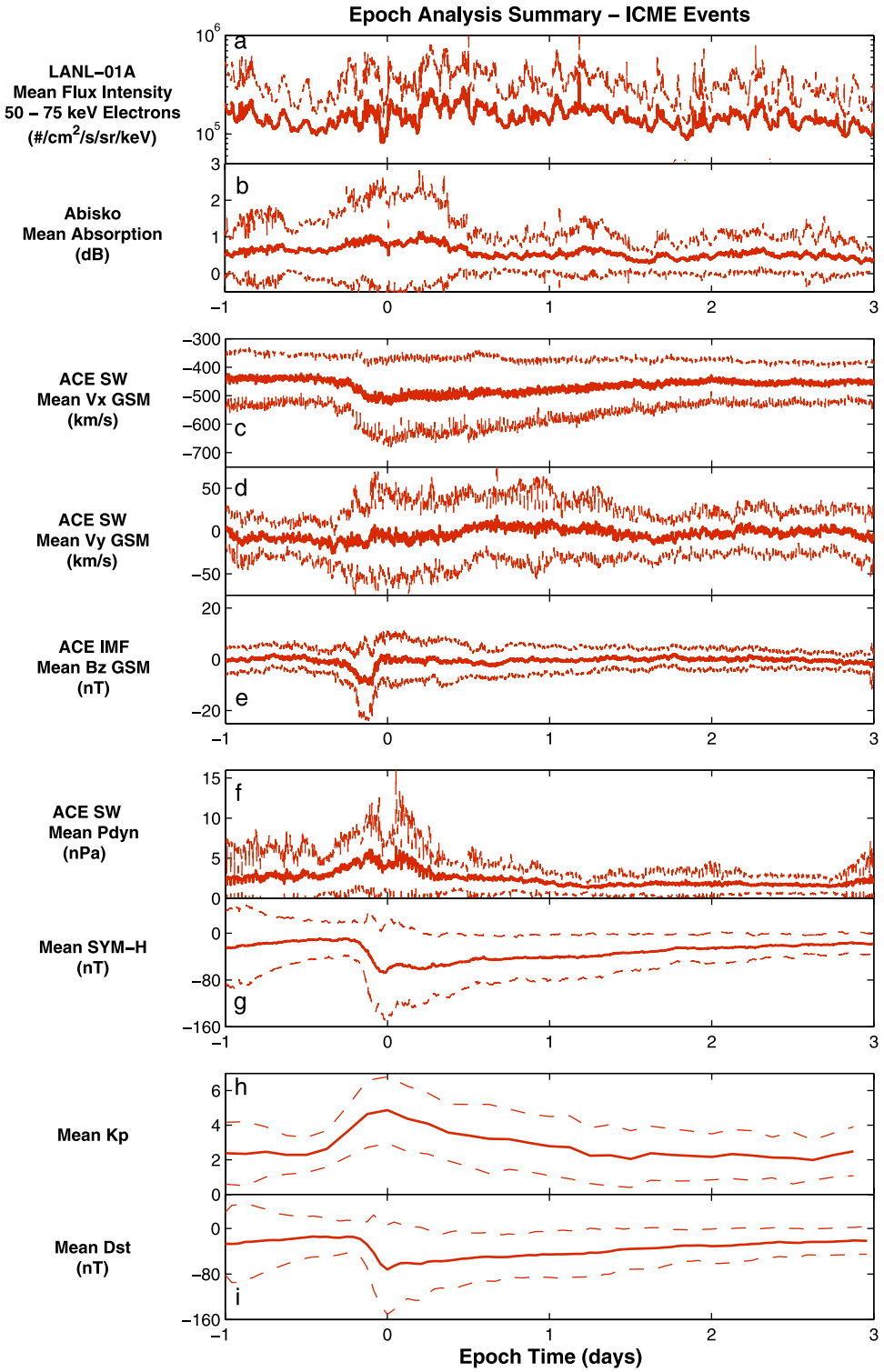

Figure 4. Superposed epoch time series of data for the set of 33 ICME-driven storms. ±1 Standard deviation from the mean is indicated for each data set. From (a) to (i), the panels show mean electron flux intensity for electrons with energies in the range 50–75 keV from the LANL-01A satellite, mean CNA from the Abisko riometer, mean solar wind velocity in the X and Y direction (GSM), mean IMF B_z (GSM), mean solar wind P_{dyn}, mean SYM-H, mean Kp and mean Dst. The zero epoch is the time of the first clear minimum in Dst for each event.

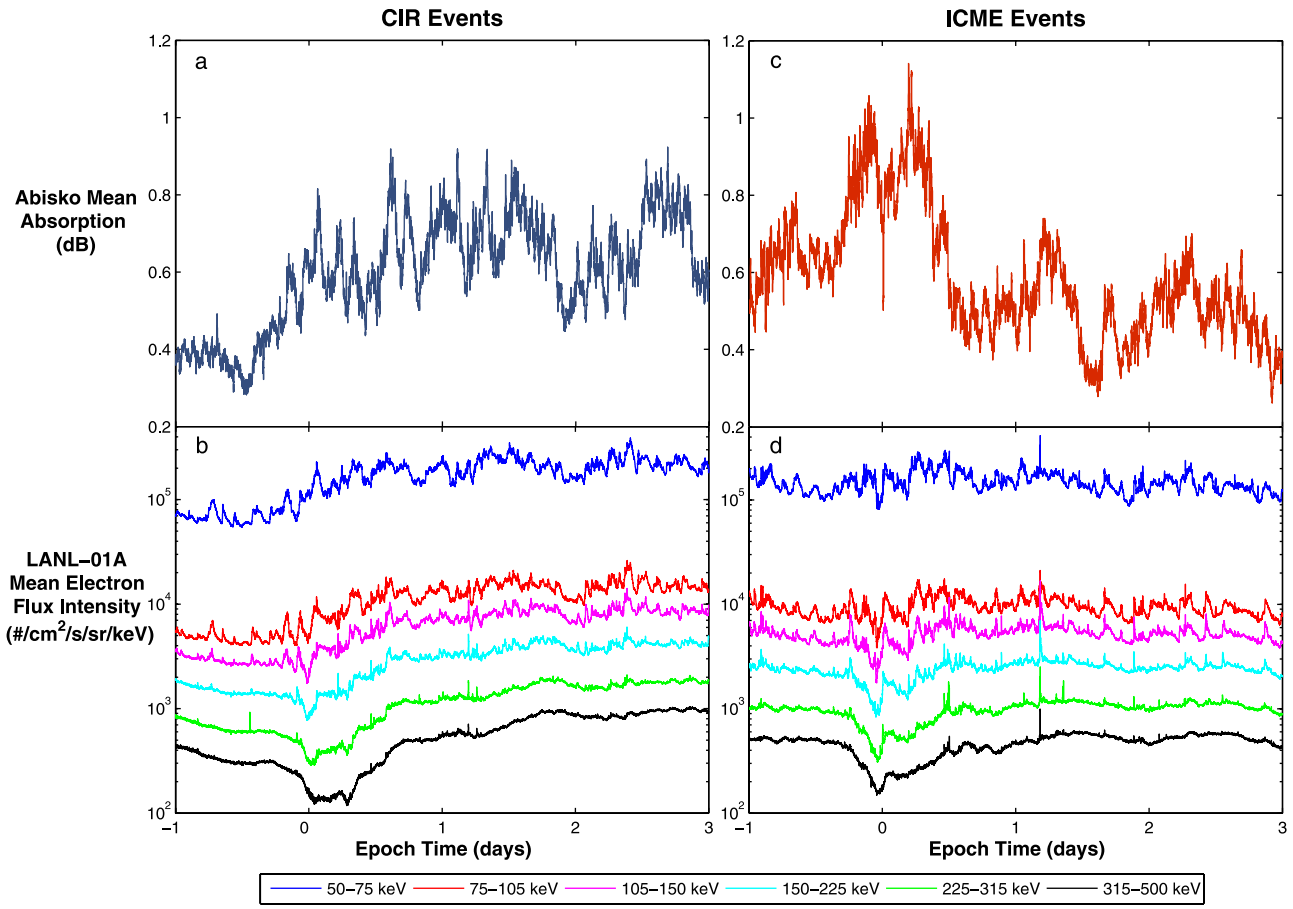

Figure 5. Superposed epoch time series of mean CNA at Abisko and mean geosynchronous electron flux intensity for electrons with energies in the range of 50–500 keV from the LANL-01A satellite. Panels (a) and (b) show the data from the set of 38 CIR-driven storms. Panels (c) and (d) show the data from the set of 33 ICME-driven storms. The zero epoch is the time of the first clear minimum in Dst for each event.

in terms of the geomagnetic field. It is possible that during geomagnetic storms the separation between the instruments exceeds the spatial extent of precipitation events.

[26] Figure 5 shows mean CNA at Abisko and mean electron flux intensity for electrons with energies in the range 50–500 keV at LANL-01A during CIR- and ICME-driven storms. Mean electron flux intensity in the higher energy channels show a similar to profile to that of the 50–75 keV channel during CIR-driven storms; relatively low flux intensity at the start of the epoch period followed by a gradual increase with the onset of activity and sustained elevation. However, the time of onset of the increase in electron flux intensity is dependent on the energy of the electrons, with higher energy channels showing an increase at a later time than the lower energy channels. The electron flux intensity profile shows lower mean flux intensity across all channels in the 50–500 keV band prior to the onset of CIR-driven storms than prior to ICME-driven storm. The signature of flux dropout is evident around the time of the zero epoch for storms driven by both structures. Flux dropouts at geosynchronous orbit have been linked to the growth phase of large geomagnetic substorms or storms altering the configuration of the magnetotail [*Moldwin et al.*, 1995]. The mean electron flux intensity during ICME-driven storms returns largely to pre-storm levels 1 to 2 days after the zero epoch. The mean flux intensity remains elevated during CIR-driven storms, not returning to pre-storm levels before the end of the epoch period (3 days). The elevation of electron flux intensity is clear in all of the energy channels shown.

[27] Typical signatures of solar wind structures can be seen in the trends in the solar wind data used in the superposed epoch study. The mean solar wind v_x (Figure 1c) steadily increases from a slow speed ($\sim$400 kms^{-1}) to higher speeds ($\sim$700 kms^{-1}) during CIR events. A rapid elevation in v_x can be seen during ICME-dominated solar wind periods just prior to the time of zero epoch, followed by a gradual return to ambient speeds. When compared to the mean solar wind velocity observed during weak and moderate ICME-driven geomagnetic storms (Figure 2c), the rapid increase around the zero epoch is not evident. This could be an indicator of IP shock activity associated with the more intense ICME-driven storms. Mean v_y (Figure 1d) is around 0 kms^{-1} during ICME-dominated solar wind. A west to east rotation is evident during CIR-dominated solar wind.

[28] The mean IMF B_z (Figure 1e) is approximately 0 nT during both ICME-driven and CIR-driven storms at all

Table 2. Summary of Descriptive Statistics of Parameters From the Set of 38 CIR-Driven Storms and 33 ICME-Driven Storms Used in the Epoch Analysis[a]

	Early Phase (−1 to +1/2 Days)									
	CIR-Driven Storms					ICME-Driven Storms				
	CNA, dB	v_x, kms^{-1}	B_z, nT	Dst, nT	Kp	CNA, dB	v_x, kms^{-1}	B_z, nT	Dst, nT	Kp
Min	−0.17	−714.05	−32.06	−109	0	−0.48	−1007.9	−78.55	−383	0
Max	4.50	−326.81	22.10	27	7	10.73	−312.94	37.97	80	9
Mean	0.48	−441.16	0.09	−11.83	2.50	0.74	−470.14	−0.94	−34.94	3.33
Median	0.34	−421.01	0.24	−5.25	2	0.43	−435.77	−0.84	−14	3
Std	0.11	19.76	0.93	4.70	0.18	0.28	22.50	2.46	14.88	0.33
	Late Phase (+1/2 to +3 Days)									
	CIR-Driven Storms					ICME-Driven Storms				
	CNA, dB	v_x, kms^{-1}	B_z, nT	Dst, nT	Kp	CNA, dB	v_x, kms^{-1}	B_z, nT	Dst, nT	Kp
Min	−0.31	−972.50	−19.87	−86	0	−0.31	−1006.40	−38.14	−182	0
Max	7.29	−363.29	20.78	30	7.3	6.15	−312.03	26.98	27	7.3
Mean	0.67	−558.20	−0.06	−23.46	3	0.49	−464.94	−0.27	−35.03	2.45
Median	0.49	−551.25	−0.05	−22.50	3	0.33	−439.85	−0.06	−22	2.15
Std	0.14	6.45	0.77	1.90	0.11	0.13	20.86	0.96	7.25	0.22

[a]Statistics are given for the early phase of each event, from −1 day to +1/2 day of the epoch, and for the later phase of each event, from +1/2 day to +3 days of the epoch.

times throughout the epoch study except immediately prior to the zero epoch, when a period of southward orientation is clear. The magnitude of the southward component for ICME-dominated solar wind is greater than for CIR-dominated solar wind during storms of all intensities, implying a greater rate of reconnection between the IMF and the magnetosphere under ICME conditions. When periods of weak and moderate storm activity only are considered (Figure 2e), the southward component has an equal magnitude for both solar wind structures allowing more meaningful comparisons to be made.

[29] Peaks in mean P_{dyn} during ICME-dominated solar wind are clear 2 to 3 h prior to the zero epoch and 1 to 2 h following the zero epoch. The initial peak occurs at the time of southward IMF. When storms of weak and moderate intensity only are considered (Figure 2f), the peaks in mean P_{dyn} become much less pronounced. During CIR-dominated solar wind, mean P_{dyn} shows a gradual increase prior to the zero epoch, around the time of the west to east rotation of the solar wind.

[30] The profiles in the mean Dst index (Figure 1f) and the mean Kp index (Figure 1g) are as expected since ICME-driven storms, on average, have a more intense signature in Dst but also show more rapid recovery. CIR-driven storms are less intense in terms of Dst and there is no real trend toward recovery within the subsequent 3 days. Peak mean Kp is greater for ICME-driven storms but mean Kp remains elevated over a longer period of time during CIR-driven storms, implying a longer period of magnetospheric convection [e.g., *Denton et al.*, 2006].

[31] Table 2 lists a summary of some of the descriptive statistics of the parameters used in this study during CIR-dominant and ICME-dominant solar wind. These parameters are taken from the data from the early phase of the storm (from −1 day to +1/2 day of the four day period) and from the later phase (from +1/2 day to +3 days of the four day period) from the 38 CIR-driven storms and the 33 ICME-driven storms used for the epoch study. From Table 2, it can be seen that the most extreme values of the parameters, including CNA, v_x and southward B_z, were observed when an ICME was the dominant structure in the solar wind and the most intense geomagnetic response, in both Dst and Kp, was driven by an ICME. The average values of these parameters in the early phase were greater during ICME-driven storms and greater range and variation in most parameters is also observed for ICME-driven storms compared to CIR-driven storms. However, in the later phase of the storms the average values of CNA, v_x and Kp are greater when CIRs are the driver of the activity. This demonstrates the persistence of activity following the onset of the storm due to the high-speed solar wind stream following the CIR. The persistence of activity is such that when data from the entire four day period of the epoch study is considered, average CNA during CIR-driven storms (∼0.60 dB) slightly exceeds that observed during ICME-driven storms (∼0.59 dB).

5. Discussion

[32] Solar wind and IMF conditions have a significant role in the occurrence and strength of auroral zone particle precipitation [e.g., *Kavanagh et al.*, 2004]. Solar wind parameters that have been linked to driving mechanisms of precipitation include velocity, southward oriented IMF [e.g., *Kavanagh et al.*, 2004] and dynamic pressure [*Brown et al.*, 1961]. In addition to a driving mechanism, a sufficient population of electrons is required for precipitation to occur [e.g., *Kavanagh et al.*, 2004]. A number of models predict the occurrence of CNA from the Kp index [e.g., *Foppiano and Bradley*, 1984, 1985; *Hargreaves*, 1966; *Kavanagh et al.*, 2004]. *Osepian and Kirkwood* [2004] found a different response in CNA driven by IP shocks based on the background level of Kp prior to the arrival of the shock.

[33] The profile of mean CNA at the Abisko riometer during the events selected for the study show that the passage of the solar wind structures drives enhanced energetic electron precipitation in the auroral zone. However, the profile in CNA differs dependent on the driving structure. In the early stages of the development of the storm, CNA is greater, on average, in ICME events. In the later stages of the storm, CNA is stronger during CIR events. It appears that the geomagnetic response to the passage of an

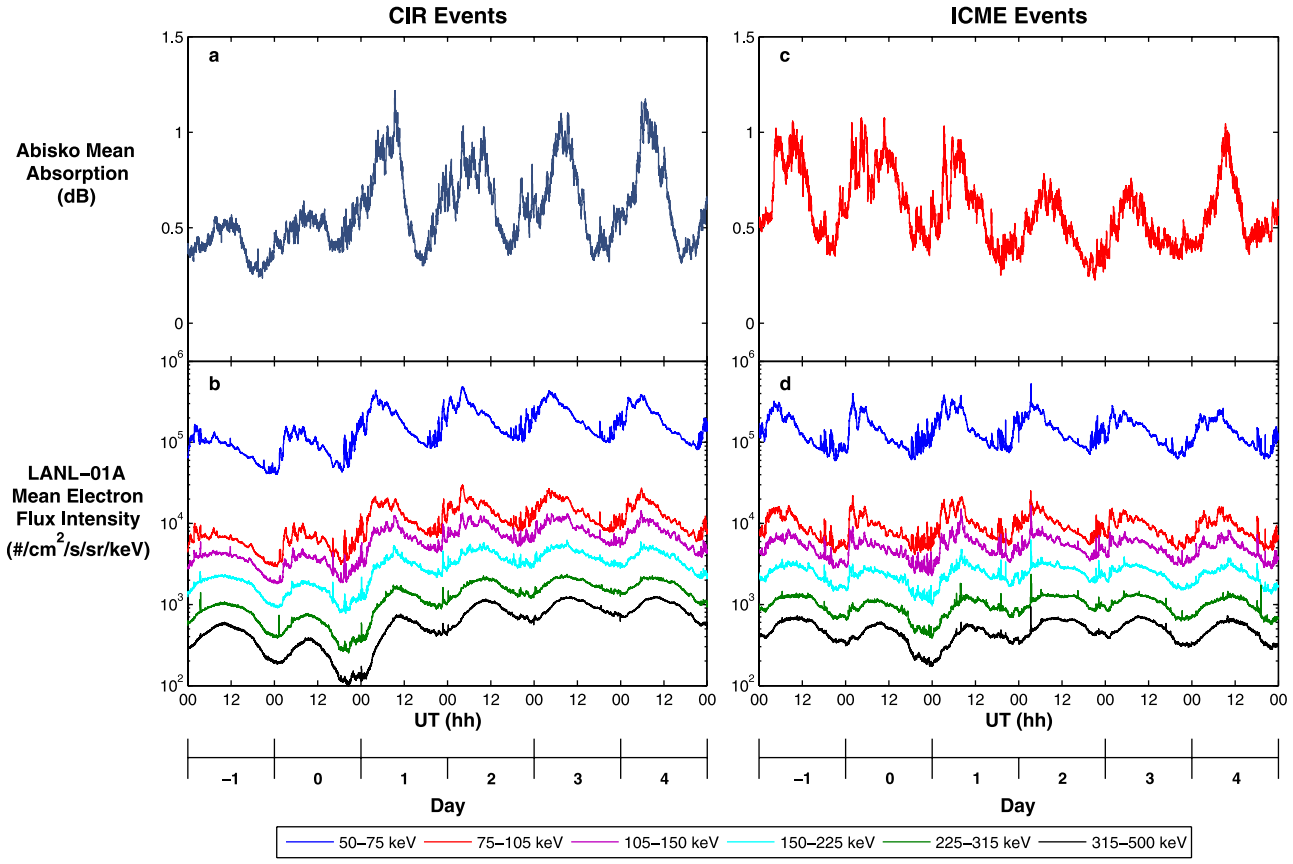

Figure 6. Time series of mean CNA at Abisko and mean geosynchronous electron flux intensity for electrons with energies in the range of 50–500 keV from the LANL-01A satellite. Panels (a) and (b) show the data from the set of 38 CIR-driven storms. Panels (c) and (d) show the data from the set of 33 ICME-driven storms. The data has been binned according to UT. Day 0 refers to the day on which storm onset occurred.

ICME is shorter than that driven by the passage of an CIR. Geomagnetic activity in the auroral zone, indicated by the Kp index, is known to remain elevated for a longer period during CIR events than during ICME events [e.g., *Denton et al.*, 2006]. This is confirmed by mean Kp in this epoch study (Figure 1f). Solar wind velocity also remains elevated due to the persistence of a high-speed stream following the compression region. This means that both enhanced geomagnetic activity and a solar wind driver for particle precipitation are provided by CIRs over a sustained period.

[34] Electron precipitation exhibits a diurnal variation [e.g., *Cowley et al.*, 1991; *Foppiano and Bradley*, 1984, 1985; *Hargreaves* 1966, 1969; *Hargreaves and Cowley*, 1967; *Hargreaves et al.*, 1987; *Hartz et al.*, 1963; *Holt et al.*, 1961; *Ranta et al.*, 1981; *Kavanagh et al.*, 2004], with a clear minimum in the local evening. Solar wind driving mechanisms appear unable to stimulate significant precipitation at this time. This has been attributed to insufficient electron flux at this local time [e.g., *Kavanagh et al.*, 2004]. The diurnal effects are largely removed from the averaged data in the epoch analysis results. Short-duration spikes in CNA, such as those driven by substorm activity in the midnight sector, can also be de-emphasized by the averaging process.

[35] To identify possible diurnal effects, Figure 6 shows mean CNA from the riometer at Abisko and mean electron flux intensity from the LANL-01A satellite during the 38 CIR-driven storms and 33 ICME-driven storms used in this study binned according to Universal Time (UT). In this figure, "Day 0" refers to the day on which storm onset occurred and is independent of the time of the first clear minimum observed in the Dst index for each event. "Day −1" is the day prior to the onset of the storm. "Day 1" to "Day 4" are the days following the onset of the storm, covering storm development and possible recovery. The magnetic local time (MLT) of the Abisko riometer is ∼UT +2 h 20 min and the MLT of the footprint of LANL-01A is ∼UT +10 min.

[36] From Figure 6, diurnal variation in CNA and electron flux intensity during both CIR-driven and ICME-driven storms is clear. During ICME events, peak CNA is consis-

tent during the first three days of the period, indicating elevated CNA prior to the onset of the storm. After the onset of storm activity, mean CNA is elevated across a wider range of local times. During the recovery phase of the storm, peak mean CNA decays. Mean geosynchronous electron flux intensity shows isolated, impulsive increases during the main phase of storm activity, including in the local evening. However, there is no significant increase in the peak mean daytime electron flux intensity with changing activity.

[37] During the CIR events, mean CNA and mean electron flux intensity are low at all local times prior to the onset of storm activity. The effect of the onset of the storm (''Day 0'') appears to have little effect on these parameters. During the development of the storm and apparent recovery, mean CNA and electron flux intensity across all energy channels in the 50–500 keV range are elevated at all local times compared to pre-storm levels. This elevation is sustained throughout the four day period considered.

[38] As CNA and geosynchronous electron flux intensity exhibit a local time dependency, the timing of the occurrence of a precipitation event may affect whether it is detected by the riometer and satellite used in this study and all precipitation events may not have been observed. Further investigation of precipitation using data from a number of riometers should provide information about the spatial extent of precipitation events and local time effects during CIR- and ICME-driven storms.

[39] *Borovsky and Steinberg* [2006] found that 67% of CIR-driven storms occurred following a period of geomagnetic calm, compared to 37% of ICME-driven storms. There is evidence of this ''calm before the storm'' in the low value of mean CNA and mean geosynchronous electron flux intensity prior to the onset of CIR-driven activity in this study. When storms of all intensities are used, an enhancement in CNA is clear for both CIR events and ICME events $\sim$ 10 h prior to the zero epoch. Before this time, mean CNA for ICME events exceeds that of mean CNA for CIR events. Additionally, mean CNA falls to a level lower than that observed initially. Higher levels of geomagnetic activity are apparent prior to the zero epoch.

[40] When storms of all intensities are considered, the peaks in CNA at Abisko during ICME-dominated solar wind occur around the time of increased in mean P_{dyn}. When weak and moderate storms only are considered, both the increased P_{dyn} and CNA are no longer pronounced. This implies that P_{dyn} is significant in the occurrence of precipitation during ICME-driven storms. When individual ICME events were investigated, impulses in P_{dyn} resulting in compression of the magnetosphere seen as impulses in the SYM-H index were identified during some events. However, it is difficult to identify instances of precipitation directly driven by impulses in P_{dyn} (sudden commencement absorption) as often the impulses occurred during a background of ongoing precipitation.

6. Conclusions

[41] The results of the epoch analysis show that there is a difference in particle precipitation during ICME-driven storms when compared to CIR-driven storms:

[42] (1) When events driving storms of all intensities are considered, mean CNA is more intense during ICME-driven storms but also shorter-lived. Mean CNA during CIR-driven storms increases gradually and remains elevated over a sustained period of time. When events driving an equivalent response in terms of storm magnitude are compared, mean CNA during CIR events is greater in magnitude as well as being sustained over a longer period, of the order of days, than mean CNA during ICME events.

[43] (2) Sustained CNA indicates the extended presence of driving mechanisms for particle precipitation during CIR-driven storms and a sufficient population of particles. Mean electron flux intensity at geosynchronous orbit for energies in the range 50–500 keV are also elevated over a sustained period during CIR-driven storms. The ''calm before the storm'' reported by *Borovsky and Steinberg* [2006] prior to the onset of CIR-driven storms is evident.

[44] (3) Of the 38 CIR events selected for analysis, 37 resulted in CIR-driven storms of weak or moderate intensity only when categorized according the Dst index. During these weak and moderate storms, a significant effect on particle precipitation was observed.

[45] **Acknowledgments.** The authors wish to thank all members of the SOPA team for providing the SOPA data. Thanks are due to D. DeLapp for providing web access to SOPA data. We would like to thank J. Manninen and the Sodankylä Geophysical Observatory for the SGO riometer data. The ACE solar wind and IMF data were obtained from the NASA CDAWeb (http://cdaweb.gsfc.nasa.gov). The Dst and Kp indices data were obtained from NOAA's Space Physics Interactive Data Resources (http://spidr.ngdc.noaa.gov). The SYM-H index data were obtained from the Kyoto World Data Center for Geomagnetism (http://swdcdb.kugi.kyoto-u.ac.jp). The authors wish to thank J. E. Borovsky, M. F. Thomsen, and A. J. Kavanagh for many helpful discussions. The authors wish to thank R. McPherron for providing his original list of CIR events.

[46] Zuyin Pu thanks Nigel Meredith and another reviewer for their assistance in evaluating this paper.

References

Baker, D. N., P. Stauning, E. W. Hones Jr., P. R. Higbie, and R. D. Belian (1981), Near-equatorial, high-resolution measurements of electron precipitation at L $\simeq$ 6.6, *J. Geophys. Res.*, *86*, 2295–2313.

Bartels, J., N. H. Heck, and H. F. Johnston (1939), The three-hour-range index measuring geomagnetic activity, *Terr. Magn. Atmos. Electr.*, *44*, 411–454.

Belian, R. D., G. R. Gisler, T. Cayton, and R. Christensen (1992), High-Z energetic particles at geosynchronous orbit during the great solar proton event series of October 1989, *J. Geophys. Res.*, *97*, 16,897–16,906.

Borovsky, J. E., and M. H. Denton (2006), Differences between CME-driven storms and CIR-driven storms, *J. Geophys. Res.*, *111*, A07S08, doi:10.1029/2005JA011447.

Borovsky, J. E., and J. T. Steinberg (2006), The ''calm before the storm'' in CIR/magnetosphere interactions: Occurrence statistics, solar wind statistics, and magnetospheric preconditioning, *J. Geophys. Res.*, *111*, A07S10, doi:10.1029/2005JA011397.

Brown, R. R., and V. M. Driatsky (1973), Further studies of ionospheric and geomagnetic effects of sudden impulses, *Planet. Space Sci.*, *21*, 1931–1935.

Brown, R. R., T. R. Hartz, B. Landmark, H. Leinbach, and J. Ortner (1961), Large-scale electron bombardment of the atmosphere at the sudden commencement of a geomagnetic storm, *J. Geophys. Res.*, *66*, 1035–1041.

Brown, R. R., H. Leinbach, S.-I. Akasofu, V. M. Driatsky, and R. J. Schmidt (1972), Quadruple conjugate pair observations of the sudden commencement absorption event on June 17, 1965, *J. Geophys. Res.*, *77*, 5602–5607.

Cane, H. V., and I. G. Richardson (2003), Interplanetary coronal mass ejections in the near-Earth solar wind during 1996–2002, *J. Geophys. Res.*, *108*(A4), 1156, doi:10.1029/2002JA009817.

Cowley, S. W. H., J. P. Morelli, and M. Lockwood (1991), Dependence of convective flows and particle precipitation in the high latitude ionosphere on the X and Z-components of the interplanetary magnetic field, *J. Geophys. Res.*, *96*, 5557–5564.

Denton, M. H., J. E. Borovsky, R. M. Skoug, M. F. Thomsen, B. Lavraud, M. G. Henderson, R. L. McPherron, J. C. Zhang, and M. W. Liemohn (2006), Geomagnetic storms driven by ICME- and CIR-dominated solar wind, *J. Geophys. Res.*, *111*, A07S07, doi:10.1029/2005JA011436.

Foppiano, A. J., and P. A. Bradley (1984), Day to day variability of riometer absorption, *J. Atmos. Terr. Phys.*, *46*, 689–696.
Foppiano, A. J., and P. A. Bradley (1985), Morphology of background auroral absorption, *J. Atmos. Terr. Phys.*, *47*, 663–674.
Gonzalez, W. D., and B. T. Tsurutani (1987), Criteria of interplanetary parameters causing intense magnetic storms (Dst < −100 nT), *Planet. Space Sci.*, *35*, 1101–1109.
Gonzalez, W., J. A. Joselyn, Y. Kamide, H. W. Kroehl, G. Rostoker, B. T. Tsurutani, and V. M. Vasyliunas (1994), What is a geomagnetic storm?, *J. Geophys. Res.*, *99*, 5771–5792.
Gonzalez, W. D., B. T. Tsurutani, and A. L. C. de Gonzalez (1999), Interplanetary origin of geomagnetic storms, *Space Sci. Rev.*, *88*, 529–562.
Gopalswamy, N. (2003), Coronal mass ejections: Initiation and detection, *Adv. Space Res.*, *31*, 869–881.
Gosling, J. T., D. J. McComas, J. L. Phillips, and J. Bame (1991), Geomagnetic activity associated with Earth passage of interplanetary shock disturbances and coronal mass ejections, *J. Geophys. Res.*, *96*, 7831–7839.
Grafe, A. (1999), Are our ideas about Dst correct?, *Ann. Geophys.*, *17*, 1–10.
Hargreaves, J. K. (1966), On the variation of auroral radio absorption with geomagnetic activity, *Planet. Space Sci.*, *14*, 991–1006.
Hargreaves, J. K. (1969), Auroral absorption of HF radio waves in the ionosphere: A review of results from the first decade of riometry, *P. IEEE*, *57*, 1348–1373.
Hargreaves, J. K., and F. C. Cowley (1967), Studies of auroral absorption events at three magnetic latitudes - I. Occurrence and statistical properties of events, *Planet. Space Sci.*, *5*, 1571–1583.
Hargreaves, J. K., H. J. A. Chivers, and W. J. Axford (1975), The development of the substorm in auroral radio absorption, *Planet. Space Sci.*, *23*, 905–911.
Hargreaves, J. K., M. T. Feeney, H. Ranta, and A. Ranta (1987), On the prediction of auroral radio absorption on the equatorial side of the absorption zone, *J. Atmos. Terr. Phys.*, *49*, 259–272.
Hartz, T. R., L. E. Montbriand, and E. L. Vogan (1963), A study of auroral absorption at 30 Mc/s, *Can. J. Phys.*, *41*, 581–595.
Holt, O., B. Landmark, and F. Lied (1961), Analysis of riometer observations obtained during polar radio blackouts, *J. Atmos. Terr. Phys.*, *23*, 229–248.
Hultqvist, B. (1966), Ionospheric absorption of cosmic radio noise, *Space Sci. Rev.*, *5*, 771–817.
Kamide, Y., N. Yokoyama, W. Gonzalez, B. T. Tsurutani, I. A. Daglis, A. Brekke, and S. Masuda (1998), Two step development of geomagnetic storms, *J. Geophys. Res.*, *103*, 6917–6921.
Kavanagh, A. J., M. J. Kosch, F. Honary, A. Senior, S. R. Marple, E. E. Woodfield, and I. W. McCrea (2004), The statistical dependence of auroral absorption on geomagnetic and solar wind parameters, *Ann. Geophys.*, *22*, 877–887.
Khan, H., and S. W. H. Cowley (1999), Observations of the response time of high-latitude ionospheric convection to variations in the interplanetary magnetic field using EISCAT and IMP-8 data, *Ann. Geophys.*, *17*, 1306–1335.
Longden, N., F. Honary, A. J. Kavanagh, and J. Manninen (2007), The driving mechanisms of particle precipitation during the moderate geomagnetic storm of 7 January 2005, *Ann. Geophys.*, *25*, 2053–2068.
Maus, S., et al. (2005), The 10th generation international geomagnetic reference field, *Phys. Earth Planet. Inter.*, *151*, 320–322.
McComas, D. J., S. J. Bame, P. Barker, W. C. Feldman, J. L. Phillips, P. Riley, and J. W. Griffee (1998), Solar Wind Electron Proton Alpha Monitor (SWEPAM) for the Advanced Composition Explorer, *Space Sci. Rev.*, *86*, 563–612.
Moldwin, M. B., M. F. Thomsen, S. J. Bame, D. J. McComas, J. Birn, G. D. Reeves, R. Nemzek, and R. D. Belian (1995), Flux dropouts of plasma and energetic particles at geosynchronous orbit during large geomagnetic storms: Entry into the lobes, *J. Geophys. Res.*, *100*, 8031–8043.
Osepian, A., and S. Kirkwood (2004), Cosmic radio-noise absorption bursts caused by solar wind shocks, *Ann. Geophys.*, *22*, 2973–2987.
Parks, G. K., R. L. Arnoldy, T. W. Lezniak, and J. R. Winckler (1968), Correlated effects of energetic electrons at the 6.6 R_E equator and the auroral zone during magnetospheric substorms, *Radio Sci.*, *3*, 715–719.
Perona, G. E. (1972), Theory on the precipitation of magnetospheric electrons at the time of sudden commencement, *J. Geophys. Res.*, *77*, 101–111.
Ranta, H., A. Ranta, P. N. Collis, and J. K. Hargreaves (1981), Development of the auroral absorption substorm: Studies of pre-onset phase and sharp onset using an extensive riometer network, *Planet. Space Sci.*, *29*, 1287–1313.
Richardson, I. G., E. W. Cliver, and H. V. Cane (2000), Sources of geomagnetic activity over the solar cycle: Relative importance of coronal mass ejections, high-speed streams, and slow solar wind, *J. Geophys. Res.*, *105*, 18,203–18,213.
Richardson, I. G., E. W. Cliver, and H. V. Cane (2001), Sources of geomagnetic storms for solar minimum and maximum conditions during 1972–2000, *Geophys. Res. Lett.*, *28*, 2567–2572.
Sheeley, N. R., Jr., R. A. Howard, M. J. Koomen, D. J. Michels, R. Schwenn, K.-H. Mühlhauser, and H. Rosenbauer (1985), Coronal mass ejections and interplanetary shocks, *J. Geophys. Res.*, *90*, 163–175.
Smith, C. W., J. L'Heureux, N. F. Ness, M. H. Acuña, L. F. Burlaga, and J. Scheifele (1998), The ACE magnetic fields experiment, *Space Sci. Rev.*, *86*, 613–632.
Spanswick, E., E. Donovan, R. Friedel, and A. Korth (2007), Ground based identification of dispersionless electron injections, *Geophys. Res. Lett.*, *34*, L03101, doi:10.1029/2006GL028329.
St. Cyr, O. C., et al. (2000), Properties of coronal mass ejections: SOHO LASCO observations from January 1996 to June 1998, *J. Geophys. Res.*, *105*, 18,169–18,185.
Stauning, P. (1996), Investigations of ionospheric radio wave absorption processes using imaging riometer techniques, *J. Atmos. Terr. Phys.*, *58*, 753–764.
Takeuchi, T., T. Araki, A. Viljanen, and J. Watermann (2002), Geomagnetic negative sudden impulses: Interplanetary causes and polarization distribution, *J. Geophys. Res.*, *107*(A7), 1096, doi:10.1029/2001JA900152.
Thomsen, M. F. (2004), Why Kp is such a good measure of magnetospheric convection, *Space Weather*, *2*, S11004, doi:10.1029/2004SW000089.
Tsurutani, B. T., W. D. Gonzalez, A. L. C. Gonzalez, F. Tang, J. K. Arballo, and M. Okada (1995), Interplanetary origin of geomagnetic activity in the declining phase of the solar cycle, *J. Geophys. Res.*, *100*, 21,717–21,733.
Tsurutani, B. T., et al. (2006), Corotating solar wind streams and recurrent geomagnetic activity: A review, *J. Geophys. Res.*, *111*, A07S01, doi:10.1029/2005JA011273.
Tsyganenko, N. A. (1995), Modeling the Earth's magnetospheric field confined within a realistic magnetopause, *J. Geophys. Res.*, *100*, 5599–5612.
Wanliss, J. A., and K. M. Showalter (2006), High-resolution global storm index: Dst versus SYM-H, *J. Geophys. Res.*, *111*, A02202, doi:10.1029/2005JA011034.

M. H. Denton, F. Honary, and N. Longden, Space Plasma Environment and Radio Science Group, Department of Communication Systems, Lancaster University, Infolab 21, Lancaster LA1 4YW, UK. (n.longden@lancaster.ac.uk)